Rheology and microrheology of deformable droplet suspensions

Rheology and microrheology of deformable droplet suspensions

M. Foglino,[a] A. N. Morozov,[a] and D. Marenduzzo[a]

Received Xth XXXXXXXXXX 20XX, Accepted Xth XXXXXXXXX 20XX
First published on the web Xth XXXXXXXXXX 200X
DOI: 10.1039/b000000x

Dense suspensions of soft colloidal particles display a broad range of physical and rheological properties which are still far from being fully understood. To elucidate the role of deformability on colloidal flow, we employ computer simulations to measure the apparent viscosity of a system of droplets of variable surface tension subjected to a pressure-driven flow. We confirm that our suspension generically undergoes discontinuous shear thinning, and determine the dependence of the onset of the discontinuity on surface tension. We find that the effective viscosity of the suspension is mainly determined by a capillary number. We present active microrheology simulations, where a single droplet is dragged through the suspension. These also show a dynamical phase transition, analogous to the one associated with discontinuous shear thinning in our interpretation. Such a transition is signalled by a discontinuity in the droplet velocity versus applied force.

1 Introduction

Emulsions are colloidal fluids with broad applications to industry and medicine, including waste treatment, food processing and pharmaceutical manufacturing [1,2].

At a microscopic scale emulsions are concentrated colloidal suspensions made of soft and deformable particles. A common example is that of blood, made of discrete and deformable red blood cells (RBCs) whose microscopic properties can affect the macroscopic rheological behaviour of the fluid [3–9]. For instance, cells affected by malaria are commonly found to be more rigid than their unaffected counterparts. In turn, this induces a distinctive rheological behaviour of the blood [10]. Thus, a better understanding of RBC flow under different conditions such as channel geometry, cell rigidity and shape is essential to develop and optimize new microfluidic devices, drug delivery techniques and even diagnosis protocol.

A suspension of deformable droplets shares some features with a hard sphere fluid, as, for instance, the viscosity increases as a function of volume fraction. However, there are also clear differences: for instance, we would expect deformability to allow different types of flow, as droplets can squeeze past each other, and the solvent can flow within them, unlike the case of hard colloids. A number of studies have been dedicated to investigate the physical properties of hard sphere fluids, shedding light on the physics of glass transition [11–13], and soft glassy rheology [14]. On the other hand, the rheological and flow properties of soft and deformable suspension [15–19] remain poorly understood. Enhancing our understanding of such systems would also open up future applications to systems with active emulsions or self-propelled droplets, whose dynamics hence rheology promises to be rich and highly non-trivial [20,21].

Previously [22], we investigated the dynamics of non-coalescing deformable droplets under pressure-driven flow by means of 2D hybrid lattice Boltzmann simulations. We showed that the emulsion rheology displays a discontinuous shear thinning behaviour, which is associated with a non-equilibrium transition (or sharp crossover) between a "hard" and a "soft" regime. The former displays slow flow, caged droplet dynamics and undeformed droplets, whereas the latter is characterised by fast flow and pronounced droplet deformation.

Having identified the origin of this rich behaviour with the extent of droplet deformability, we are now interested in characterising the rheological properties as a function of the droplets surface tension. To this end, we perform hybrid lattice Boltzmann simulations of 2D emulsions in which we vary both the external pressure gradient and the softness of the particles. We show that the non-equilibrium hard-soft transition (i.e., the point of discontinuous shear thinning) is progressively shifted towards higher values of the applied pressure-difference as we increase the droplet surface tension and we find that the apparent viscosity is predominantly determined by the capillary number of the system.

To further characterise the hard-soft transition, we perform simulations inspired by typical active microrheology measurements [23–26], where one of the droplets is selected and dragged through the suspension. This strategy enables us to study the response of the system to a localised perturbation, and we identify a discontinuous behaviour in the probe velocity with intriguing analogies to the sudden decay in viscosity displayed by the bulk.

Whilst the model presented in this work may be directly

[a] *SUPA, School of Physics and Astronomy, University of Edinburgh, Edinburgh EH9 3FD, UK*

recreated in the lab via suspensions of deformable and non-coalescing droplets (e.g., stabilised by a surfactant), we suggest that it could also be used to qualitatively describe the flow properties of red blood cells or other eukaryotic cells.

2 Model and Methods

Our aim here is to investigate numerically the rheological properties of a two-dimensional suspension of non-coalescing deformable droplets subjected to a pressure-driven flow. Our simulations allow us to tune the following three key parameters which determine the flow properties of our suspension: (i) the pressure difference ΔP causing the flow, (ii) the suspension area fraction Φ, defined as the ratio between the area of all droplets and the total area of the simulation domain, and (iii) the surface tension γ which accounts for the droplets deformability.

Our soft droplet suspensions are described by introducing a set of phase-fields ϕ_i, $i = 1,\ldots,N$, where N is the total number of droplets. The fact that we use a different phase field for each droplet ensures that they are non-coalescing. On the other hand, the underlying fluid flow is described by a velocity field $\mathbf{v}$.

Our suspension equilibrium behaviour is described by the following free energy density:

$$f = \frac{\alpha}{4}\sum_i^N \phi_i^2(\phi_i-\phi_0)^2 + \frac{K}{2}\sum_i^N(\nabla\phi_i)^2 + \varepsilon\sum_{i,j,i<j}\phi_i\phi_j. \quad (1)$$

The first term in Eq. (1) ensures stability of each of the droplets, by creating two coexisting minima for $\phi=\phi_0$ and $\phi=0$. These two minima represent the inside and outside area of the i-th droplet respectively. The droplets deformability properties are determined by their surface tension $\gamma = \sqrt{8K\alpha/9}$ and can therefore be tuned, for instance, by changing the value of the constant K. For simplicity, from now on we will refer to the latter quantity K as the surface tension-like parameter. The parameters K and α also determine the interfacial thickness as $\xi = \sqrt{2K/\alpha}$. The last term in the free energy density introduces a soft repulsion between droplets – its strength is measured by the constant $\varepsilon > 0$. This soft repulsion term prevents droplet overlap in dense suspensions – we do not expect its exact value to qualitatively affect our findings.

The dynamics of the droplets is described by a set of Cahn-Hilliard equations for the phase fields ϕ_i:

$$\frac{\partial\phi_i}{\partial t} + \nabla\cdot(\mathbf{v}\phi_i) = M\nabla^2\mu_i, \quad (2)$$

where M represents the mobility and $\mu_i = \partial f/\partial\phi_i - \partial_\alpha f/\partial(\partial_\alpha\phi)$ is the chemical potential of the i-th droplet. This set of equation conserves the area of each droplets.

The droplets dynamics is coupled to that of the underlying solvent trough the fluid velocity field $\mathbf{v}$ which evolves according to the Navier-Stokes equation:

$$\rho\Big(\frac{\partial}{\partial t} + \mathbf{v}\cdot\nabla\Big)\mathbf{v} = -\nabla p - \sum_i \phi_i\nabla\mu_i + \eta_0\nabla^2\mathbf{v}, \quad (3)$$

where ρ indicates the fluid density, p denotes its pressure and η_0 the viscosity of the underlying solvent. The term $\sum_i \phi_i\nabla\mu_i$, which can be expressed as a divergence of a stress tensor, represents the internal forces due to the presence of non-trivial compositional order parameters which vary spatially.

We analyse the dynamics of the system by means of hybrid lattice Boltzmann simulations (LB)[27,28], where Eq. (3) is solved through the lattice Boltzmann algorithm while Eq. (2) is addressed using a finite difference method.

In our simulations, the soft droplets suspension is subjected to a constant external pressure gradient acting on the underlying fluid, and causing the system to flow (in a Newtonian fluid, this setup leads to Poiseuille flow with a parabolic velocity profile). In order to simulate a pressure gradient, a body force (force per unit density) was included in our LB algorithm, and added to the collision operator at each lattice node. The term $\sum_i \phi_i\nabla\mu_i$ was also added as a body force, as this procedure limits the spurious LB velocities in equilibrium[29]. Our simulations are run on a 96×96 lattice, with periodic boundary conditions along the x axis , and boundary walls along the y axis. Neutral wetting conditions were used, as they create a layer of boundary droplets which slow down the motion of those which come into contact with them. These were enforced by requiring that, for each $i = 1,...,N$,

$$\frac{\partial\mu_i}{\partial z} = 0, \qquad \frac{\partial\nabla^2\phi_i}{\partial z} = 0. \quad (4)$$

In Eq.(4), the first condition ensures density conservation (no flux boundary), while the second one determines the wetting to be neutral, i.e. the droplets at the boundary form an angle of 90° with the wall surface.

The parameters used in our simulations are the following. We fix the droplet radius to $r = 8$ and the mobility to $M = 0.1$, while the free energy parameters are $\alpha = 0.07$, $\varepsilon = 0.05$, and K varies within the range $[0.02 - 0.25]$. The viscosity of the underlying fluid is $\eta_0 = \frac{5}{3}$ (for simplicity this is also the viscosity of the fluid inside the droplets), and the value of applied pressure difference varies within the range $[10^{-5} - 10^{-4}]$. While the trends that we show in our results section are generic and do not rely on a particular choice of physical unit, the parameters listed above can be mapped onto a physical system with droplets of size (diameter) equal to $100\mu m$, in a background fluid with viscosity $10^{-2}Pas$ (in the absence of droplets), and where the surface tension $\gamma = \sqrt{(8K\alpha)/9} \sim 0.09$ corresponds to $1mN/m$. With this mapping, a velocity of

10^{-3} in simulation units corresponds to $1mm/s$. The Reynolds number, calculated as $Re = \frac{\rho v_{max} L}{\eta_0}$ where ρ is the density, L the system size , v_{max} the maximum value of the droplets' velocity and η_0 the viscosity of the underlying fluid, ranges from ~ 0.04 ($\Delta P = 5 \times 10^{-5}$, resulting in a fluid maximum velocity $v_{max} \sim 0.03$) to ~ 8 (for $\Delta P = 10^{-4}, v_{max} \sim 0.07$). These values are always small enough that no inertial instabilities are observed. The conventional Capillary number $Ca = \frac{\eta_0 v}{\gamma}$ ranges from ~ 0.06 (for $\Delta P = 5 \times 10^{-5}$) to ~ 1.23 (for $\Delta P = 10^{-4}$).

3 Results

3.1 Pressure-driven flow

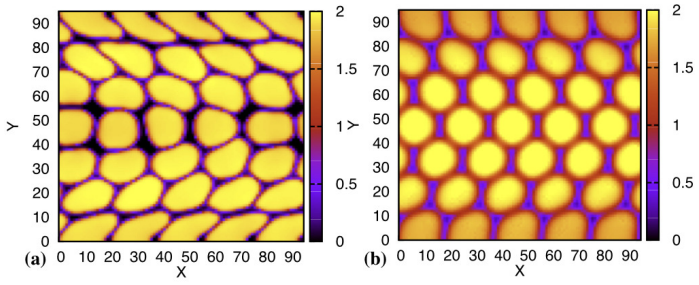

Fig. 1 ((**a**) Snapshot of the simulation of a suspension of $\Phi = 76.3\%$, $K = 0.02$ subjected to a pressure difference $\Delta P = 7 \times 10^{-5}$.(**b**) Snapshot of the simulation of a suspension of $\Phi = 76.3\%$, $K = 0.18$ subjected to a pressure difference $\Delta P = 7 \times 10^{-5}$. It can be seen that lower values of K lead to a softer foam, with more pronounced droplet deformations.

In this work we aim to understand and characterise the role of droplet deformability in determining the flowing properties of the overall suspension. To this end, we perform two-dimensional simulations of a suspension of deformable droplets in a liquid medium, subjected to a pressure-driven flow, where we systematically vary the values of droplet surface tension K and applied pressure difference ΔP. A first feel for the extent to which surface tension can affect the behaviour of the system comes from inspection of Fig. 1, where the simulation snapshots for two different values of K display a remarkable qualitative difference.

To quantitatively characterise the rheological behaviour of our suspension, we measure the throughput flow in our simulations, $Q = \int dy v_x(y)$, and use it to define an effective viscosity $\eta_{eff} = \frac{\eta}{\eta_0}$, where η_0 is the viscosity of the underlying fluid. This effective viscosity is defined as the ratio between the throughput flow in a Newtonian fluid with viscosity η_0 and Q. As shown in Fig. 2**(a)** and **(b)**, η_{eff} undergoes a discontinuous shear thinning behaviour both as a function of applied pressure difference ΔP and surface tension-like parameter K. Additionally, the various viscosity curves in Fig. 2**(a)**, referring to different values of the surface tension-like parameter K, show that the value of the applied ΔP corresponding to the discontinuous shear thinning progressively shifts towards higher values as K is increased.

This discontinuous shear thinning behaviour, as discussed in our previous work[22], is a result of the system transition between a "hard" and a "soft" phase. While the former is characterised by almost spherical droplets which tend to resist deformation and flow very slowly, the latter is associated with droplets that are more susceptible to deformation and therefore flow more easily. Such an interpretation is in agreement with the observed shift of the pressure difference corresponding to the viscosity jump, ΔP_{jump}, as a function of K shown in Fig. 2**(c)**. Higher values of K cause the suspension to be overall less deformable, and we therefore expect the transition towards the soft phase to occur for progressively larger values of applied pressure difference, as larger forces are needed to create droplet deformations. We can use a similar argument to explain the behaviour observed in Fig. 2**(b)** where the suspension viscosity is now plotted as a function of K for different fixed value of applied pressure difference ΔP. In this case, increasing K takes the system from the soft to the hard phase, so that the viscosity sharply increases. The jump in the suspension effective viscosity shifts towards higher K values as we increase the applied ΔP, as the latter parameter favours the soft phase. Additionally, increasing ΔP leads to overall smaller effective viscosities, as the system is shear thinning.

We found empirically that within the parameter range the shape of the viscosity curves is predominantly determined by the following capillary number,

$$Ca = \frac{\Delta P}{K} L r^2 \tag{5}$$

where r is the droplet radius and L is the system size. Of all functional forms of the type $\frac{\Delta P}{K} L^n r^{(3-n)}$ with n integer, this is the combination which we empirically found leads to the best collapse. * Note that, while this ratio still measures the relative contribution of viscous and interfacial forces, the latter are now proportional to K, the term which enters the free energy density, rather than $\sqrt{K}$ as in the conventional definition of the capillary number (given above). The fitness of such a capillary number as a key parameter describing the rheological properties of our suspension is demonstrated by Fig. 2**(c)** and **(d)**, where the effective viscosity curves referring to different values of fixed droplet surface tension are plotted as a function of Ca. As is apparent from a comparison between

* While simulations in the main text have been performed with $\alpha = 0.07$, we have also performed simulations at three other values of α. Whilst this parameter does not enter the capillary number, it can still affect the viscosity curves as, for instance, increasing it leads to a decrease in the interfacial thickness of the droplets, hence to a decrease in the effective area fraction and, therefore, in the viscosity.

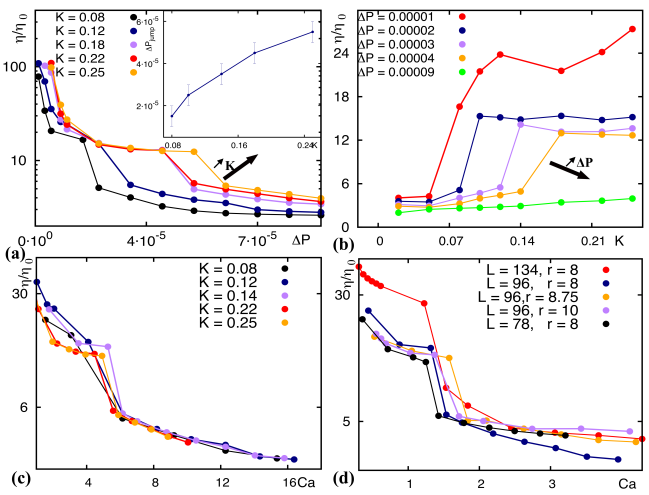

Fig. 2 **(a)**Plot of the suspension effective viscosity η_{eff} as a function of the applied pressure difference for a system of area fraction $\Phi = 65.4\%$ and different fixed values of the surface tension-like parameter K. **Inset** Plot of the values of ΔP corresponding the the viscosity drop as a function of K.**(b)**Plot of η_{eff} as a function of the surface tension-like parameter K for a system of area fraction $\Phi = 65.4\%$ and different fixed values of the applied pressure difference ΔP. **(c)**Plot of the suspension effective viscosity as a function of the system Capillary number Ca for a system of area fraction $\Phi = 65.4\%$ and different fixed values of K. Comparing **(c)** with **(a)**, we can notice that the various viscosity curves collapse onto a single one if they are plotted as a function of Ca instead of ΔP. **(d)** Plot of the suspension effective viscosity as a function of the Capillary number Ca for a system of area fraction $\Phi = 64.5\%$ and different fixed values of the droplet radius r and system size L. The scaling is compatible with r^2L.

Fig. 2**(a)** and **(c)**, the viscosity curves for different values of K all approximately collapse on the same master curve as we plot them against the Capillary number (instead of the simple applied pressure difference ΔP). This is in line with the results obtained in[6] for simulations of red blood cell rheology, within a model exhibiting continuous shear thinning. Moreover, Fig. 2**(d)** shows that the suspension viscosity curves display a scaling with Ca proportional to r^2L. We therefore conclude that the Capillary number is the appropriate control parameter for describing the elastic and flow properties of our suspension.

Having performed simulations for a variety of different parameters, we are now able to draw a phase diagram describing the transition between the soft and hard phase of our system. As previously explained, the transition between these two phases is marked by a sudden drop in the suspension effective viscosity for a certain threshold of applied pressure difference. We therefore label as "soft" all the cases where the value of viscosity is "low" – i.e., corresponding to the right

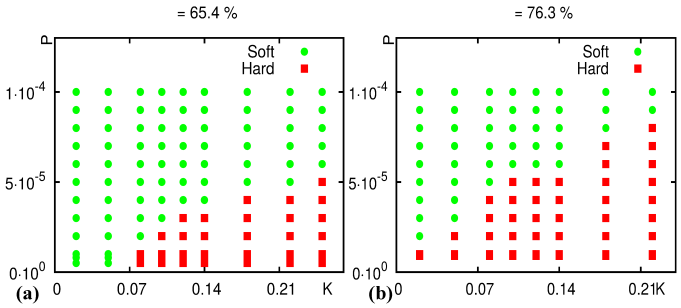

Fig. 3 **(a)**Phase diagram for a suspension of area fraction $\Phi = 65.4\%$ obtained through simulations performed over different values of surface tension-like parameter K and applied pressure difference ΔP. The green area represents the soft phase of our suspension, while the red one corresponds to the hard regime.**(b)**Phase diagram as in **(a)** for a system of area fraction $\Phi = 76.3\%$.

branch of the viscosity curve, following the downward jump corresponding to discontinuous shear thinning (see Fig. 2**(a)**). On the other hand, all the cases belonging to the left branch of the viscosity curve – i.e., to higher values of η_{eff} – are labelled as "hard". In Fig. 3 we plot two phase diagrams corresponding to different values of the suspension area fraction Φ, with increasing values of the surface tension-like parameter on the x axis, and of the applied pressure difference on the y axis. The green and red area corresponds to the soft and hard regime, respectively. As expected intuitively, as we move along the $x-$axis – i.e., increasing K and keeping fixed ΔP – our system switches from the soft towards the hard phase. On the other hand, moving along the y axis – i.e., increasing ΔP keeping the value of K fixed – droplet deformation increases and the suspension undergoes a hard-to-soft transition.

The comparison between Fig. 3**(a)** and **(b)** additionally suggests that the area fraction Φ affects the overall stability of the soft and hard phases. Thus, for the lower Φ the soft phase is predominant (green area in Fig. 3**(a)**), whereas for the larger Φ the range of stability of the hard phase increases in size (red area in Fig. 3**(b)**). This is because increasing Φ promotes jamming and a solid-like (hence hard) behaviour. Note that this is true despite the fact that at large Φ particles are frequently non-circular: what is important for the hard phase to be stable is that subsequent time-dependent deformations from this ground state are unlikely.

3.2 Micro-rheology

We now discuss a different set of simulations, this time modelling a microrheology experiment. Such experiments analyse the dynamics of a single probe particle, or droplet, which is

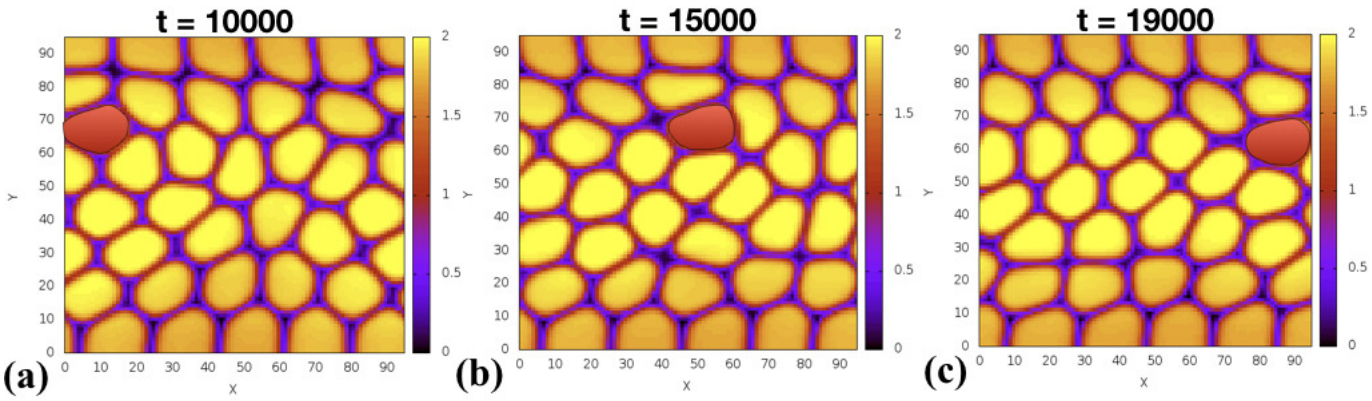

Fig. 4 Snapshots from a simulation of active micro-rheology. The red droplet (the colour of the probe droplet has been manually modified in order to mark it, the actual value of ϕ is 2 like all the other droplets) is the probe which moves due to the applied body-force $f = 6 \cdot 10^{-5}$. Snapshots **(a)**, **(b)** and **(c)** are taken from the same simulation and refer to different timesteps (namely $t = 10000, 15000$ and $t = 19000$). As we can notice, the probe droplet travels across the entire simulation box within 9000 timesteps.

immersed in a suspension. This setup makes it possible to extract some rheological properties of the overall suspension avoiding the limitation of a bulk rheology measurement (such as the required big sample size).

Here we focus on the case of *active* microrheology, where one of the droplets is selected and dragged through the suspension – we call this the 'probe' droplet. To simulate this case, we apply a spatially dependent body-force to the system – along the horizontal direction in Fig. 4. This body force is modulated by the phase field of the probe droplet via the term $\sum_i \phi_i \nabla \mu_i$ of Eq. (3). Selecting only the phase field ϕ_i of the i-th droplet, we apply the forcing only on the probe droplet, forcing its motion through the suspension. We then monitor how the dynamics of the probe droplet is affected by Φ, K and the magnitude of the force (more precisely, its maximum over space) which we refer to as f. While in our previous analysis, the pivotal quantity used to characterise the suspension rheological properties was its effective viscosity, we now study how the (steady state) probe velocity changes with parameters. Remarkably, we find that discontinuous shear thinning leaves a detectable signature in microrheology measurements as well. Thus, as shown in Fig. 6, we observe a discontinuous behaviour in the curve portraying the probe velocity curve as a function of the applied body-force. In analogy with the discontinuity in the effective viscosity, the jump in the probe velocity signals a transition from a hard, solid-like, regime, to a soft, liquid-like, one. For low values of f the probe struggles to move steadily, and is in practice trapped by its neighbouring droplets. On the other hand, there is a critical threshold of f after which the probe droplet is able to move much more easily across the suspension, as it can deform more readily to squeeze past the other droplets in the suspension. The solvent flow patterns either side of the threshold are very different (Fig. 5). For $f < f_c$ the flow field does not penetrate the droplets, and is only marginally enhanced within or near the probe droplets. For $f > f_c$, the solvent flow is larger within droplets, is fast within the probe droplet and rapidly decays outside it.

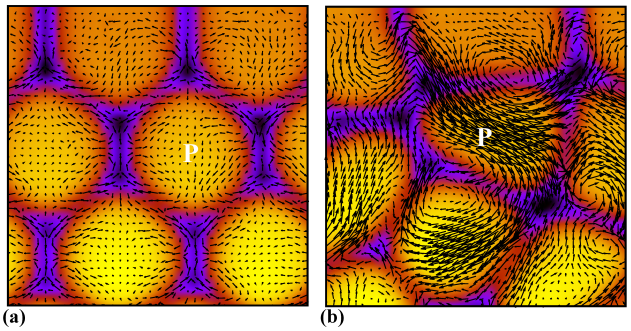

Fig. 5 (a) Flow field patterns in the vicinity of the probe droplet (denoted via P) for $f < f_c$. **(b)** Same for $f > f_c$. In both snapshots, the probe droplets is labelled with the letter **P**.

As discussed in the previous section, in a mascroscopic flow setup, the location of the hard-to-soft transition can be tuned by the value of the droplet surface tension-like parameter K, as demonstrated by the progressive shift of the viscosity discontinuity towards higher values of pressure difference as K is increased. Is a similar effect seen in microrheology? To address this question, we analysed how the location of the discontinuity in the probe droplet velocity is affected by changes in K. The results of these simulations, presented in Fig. 6, show that the discontinuity occurs for progressively larger values of the

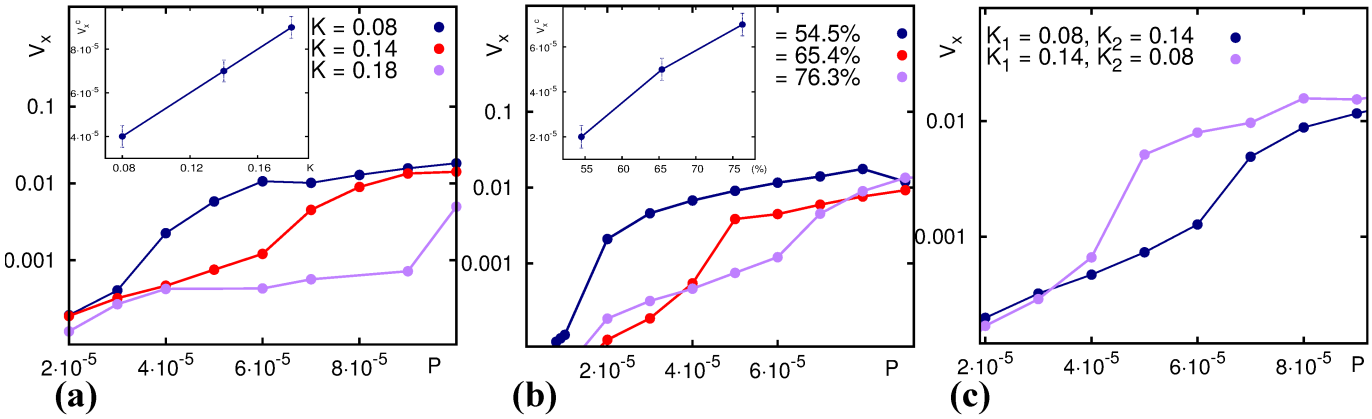

Fig. 6 (a) Probe droplet velocity curves as a function of the applied forcing for a suspension area fraction of $\Phi = 76.3\%$. The three curves refer to different values of the surface tension-like parameter, namely $K = 0.08$, $K = 0.14$ and $K = 0.18$. As we can notice, the jump in the probe droplet velocity is progressively shifted towards higher values of the forcing as K is increased. **Inset** Plot of the threshold value of the forcing, associted with the velocity discontinuity, as a function of K. **(b)** Probe droplet velocity curves as a function of the applied forcing for a suspension of surface tension $K = 0.14$. The three curves refer to different values of the suspension area fraction, namely $\phi = 54.5\%$, $\phi = 65.4\%$ and $\phi = 76.3\%$. **Inset** Plot of the threshold value of the forcing which is associated with the velocity discontinuity as a function of the suspension area fraction. **(c)** Probe droplet velocity curves as a function of the applied forcing for a suspension of area fraction $\phi = 76.3\%$ for different values of the surface tension-like parameter. In these simulations, the probe is characterised by a different K (K_1) with respect to the rest of the rest of the droplets (K_2). The purple curve refers to the case where the we simulate a "hard" probe moving across a "soft" suspension, while the blue one correspond to the opposite case.

applied forcing as we increase the value of K. In agreement with our previous macroscopic flow results, the transition from the hard to the soft phase becomes more "difficult" for suspensions with stiffer droplets: i.e., in order to reach the soft phase a higher value of ΔP is needed. In the inset of Figs.6**(a)** and **(b)** we show the value of the forcing correspondent to the jump in the probe velocity as a function of the surface tension and area fraction, respectively. As can be seen, this value increases near-linearly as a function of both parameters, and increasing either K or Φ favours the hard phase.

Finally, we performed simulations where we set different values for the surface tension of the probe droplet and the rest of the droplets in the suspension. The rationale for doing so is to investigate whether the physical features of the probe affect our measurements, and in particular our estimate for the threshold forcing needed to trigger the transition to the soft phase. For an ideal active microrheological experiments, the terminal velocity of the probe should be determined by the Stokes law, hence only depend on probe size and medium effective viscosity (where the latter should ideally be probe-independent).

We considered two cases: (i) one in which case a soft probe is dragged across a suspension of more rigid droplets, and (ii) the opposite scenario where a hard probe moves within a more deformable environment. As shown in Fig. 6**(c)**, these two complementary cases yield a different threshold for the forcing which triggers the hard-to-soft transition. When a soft probe ($K_1 = 0.08$) is immersed in a more rigid suspension ($K_2 = 0.14$), the transition occurs for a value of f which is indistinguishable from that obtained previously for the case of homogeneous $K = 0.14$ ($f = 7 \cdot 10^{-5}$). When considering a rigid probe ($K_1 = 0.14$) moving across a softer suspension ($K_2 = 0.08$), the threshold of the forcing shifts towards a lower value ($f = 5 \cdot 10^{-5}$), again suggesting a similar behaviour to the overall soft suspension case with homogeneous surface tension-like parameter, now $K = 0.08$. Our results therefore suggest that, within our microrheology set-up, the details of the probe do not significantly affect the measurements, and in particular the estimate of the hard-to-soft transition point – the droplet being dragged therefore behave as an ideal microrheological probe in this respect.

4 Conclusions

In summary, we presented here two dimensional lattice Boltzmann simulations of a system of non-coalescing, deformable droplet suspension where the role of droplet surface tension and deformability are investigated. Applying a pressure-driven macroscopic flow, we observe that the rheology of our system entails a discontinuous shear thinning behaviour, which is associated with a non-equilibrium phase transition (or very sharp crossover) between a hard phase, which flows

slowly, and a soft phase, where more frequent droplet deformations lead to a faster flow. In order to test the effect of droplet deformability more systematically, we performed a set of simulations where we study the behaviour of the system (effective viscosity) as a function of both the applied pressure difference as well as the droplet surface tension. Our results show that the observed hard-soft transition progressively shifts towards higher values of applied pressure difference as we increase the droplet surface tension. In other words as shown in Fig.2**(a)** and Fig. 3, a more rigid system (high values of K) requires a higher threshold value of the applied pressure difference to trigger its transition towards the soft phase.

Notably, we found that the rheological properties of our suspension are mainly determined by its capillary number Ca, defined for our system as in (5). This parameter, which captures the interplay between the surface tension and external flow, can be used to approximately collapse all the flow (viscosity) curves onto a single master curve, as shown in Fig. 2**(c)**. This suggests that Ca is the main parameter determining the macroscopic flow of our suspensions.

Finally, we performed active microrheology simulations, where a single probe droplet is dragged across the overall suspension. By varying the value of the body force applied to the probe, we observed a discontinuous behaviour in its steady state (terminal) velocity. This discontinuity is the analogue of the sharp viscosity drop observed in our macroscopic flow simulations, and corresponds to a sharp decrease in the effective friction felt by the probe droplet. We interpret this phenomenon as another signature of the nonequilibrium hard-to-soft transition that our suspension undergoes.

We thank Davide Michieletto for numerous useful discussions, and we acknowledge ERC (COLLDENSE Network) for funding.

References

1 R. G. Larson, *The structure and Rheolgy of Complex Fluids*, Oxford University Press, 1999.

2 R. A. L. Jones, *Soft Condensed Matter*, Oxford University Press, 2002.

3 M. O.K.Baskurt, M.Hardeman and H.J.Meiselman, *Handbook of Hemorheology and Hemodynamics*, IOP Press, Amsterdam, Netherlands, 2007.

4 D. A. F. Kathrin Mller and G. Gompper, *Sci. Rep.*, 2014, **4**,.

5 H. Zhao and E. S. G. Shaqfeh, *Phys. Rev. E*, 2011, **83**, 061924.

6 G. R. Lazaro, A. Hernandez-Machado and I. Pagonabarraga, *Soft Matter*, 2014, **10**, 7195–7206.

7 D. A. Fedosov, M. Peltomki and G. Gompper, *Soft Matter*, 2014, **10**, 4258–4267.

8 T. Ye, N. Phan-Thien and C. T. Lim, *Journal of Biomechanics*, 2016, **49**, 2255 – 2266.

9 J. Mauer, S. Mendez, L. Lanotte, F. Nicoud, M. Abkarian, G. Gompper and D. A. Fedosov, *Phys. Rev. Lett.*, 2018, **121**, 118103.

10 D. A. Fedosov, B. Caswell, S. Suresh and G. E. Karniadakis, *Proceedings of the National Academy of Sciences*, 2011, **108**, 35–39.

11 C. Holmes, M. Cates, M. Fuchs and P. Sollich, *J. Rheol.*, 2005, **49**, 237 – 269.

12 G. L. Hunter and E. R. Weeks, *Reports on Progress in Physics*, 2012, **75**, 066501.

13 P. N. Pusey, E. Zaccarelli, C. Valeriani, E. Sanz, W. C. K. Poon and M. E. Cates, *Phil. Trans. R. Soc. A*, 2009, **367**, 4993–5011.

14 S. M. Fielding, M. E. Cates and P. Sollich, *Soft Matter*, 2009, **5**, 2378–2382.

15 H. Zhou and C. Pozrikidis, *Phys. Fluids*, 1994, **6**, 80.

16 A. Nourbakhsh, S. Mortazavi and Y. Afshar, *Phys. Fluids*, 2011, **23**, 123303.

17 A. Z. Zinchenko and R. H. Davis, *J. Fluid Mech.*, 2015, **779**, 197–244.

18 A. Z. Zinchenko and R. H. Davis, *J. Fluid Mech.*, 2017, **816**, 661–704.

19 M. Loewenberg and E. J. Hinch, *J. Fluid Mech.*, 1996, **321**, 395–419.

20 F. Fadda, G. Gonnella, A. Lamura and A. Tiribocchi, *The European Physical Journal E*, 2017, **40**, 112.

21 G. Negro, L. Carenza, P. Digregorio, G. Gonnella and A. Lamura.

22 M. Foglino, A. N. Morozov, O. Henrich and D. Marenduzzo, *Phys. Rev. Lett.*, 2017, **119**, 208002.

23 L. G. Wilson and W. C. K. Poon, *Phys. Chem. Chem. Phys.*, 2011, **13**, 10617–10630.

24 L. Mohan, M. Cloitre and R. T. Bonnecaze, *J. Rheol.*, 2014, **58**, 1465–1482.

25 T. Gisler and D. A. Weitz, *Current Opinion in Colloid and Interface Science*, 1998, **3**, 586 – 592.

26 E. B. Vadas, H. L. Goldsmith and S. G. Mason, *Transactions of the Society of Rheology*, 1976, **20**, 373–407.

27 A. Tiribocchi, N. Stella, G. Gonnella and A. Lamura, *Phys. Rev. E*, 2009, **80**, 026701.

28 M. R. Swift, E. Orlandini, W. R. Osborn and J. M. Yeomans, *Phys. Rev. E*, 1996, **54**, 5041–5052.

29 A. J. Wagner, *Int. J. Mod. Phys. B*, 2003, **17**, 193–196.